Research Square

Preprints are preliminary reports that have not undergone peer review.
They should not be considered conclusive, used to inform clinical practice,
or referenced by the media as validated information.

Mechanical and corrosion characteristics of 6061-T6 Aluminum alloy samples reinforced with alumina micro and nanoparticles fabricated by Friction Stir Processing

Ramin Karami (RaminKarami.UrmiaUN@yahoo.com)
Department of Mechanical Engineering, Faculty of Engineering, Urmia University, Urmia, Iran
Mir Ali Asghar Abdollahi
Department of Mechanical Engineering, Faculty of Engineering, Urmia University, Urmia, Iran
https://orcid.org/0000-0001-8233-6074

Research Article

Keywords: Alumina Powder, Friction Stir Processing, Nanocomposite, Fractography, potentiodynamic polarization test

Posted Date: April 19th, 2022

DOI: https://doi.org/10.21203/rs.3.rs-1561029/v2

License: This work is licensed under a Creative Commons Attribution 4.0 International License.
Read Full License

Version of Record: A version of this preprint was published at Proceedings of the Institution of Mechanical Engineers, Part C: Journal of Mechanical Engineering Science on January 30th, 2023. See the published version at https://doi.org/10.1177/09544062231152998.

Abstract

The present study investigates the mechanical and corrosion properties of reinforced 6061TT6 Aluminum samples after friction stir processing. Three different composites are fabricated: one without any powder and the others with micrometer and nanometer alumina powder (h) as reinforcing particles. The hardness, tensile, and Potentiodynamic polarization tests are performed to compare the new samples with the base metal. The results show that friction stir processing has increased the tensile and ultimate strength of the composites by an average of 181 % compared to the base metal. The strength of the composites with additives is significantly affected by the size of the particles. The hardness of the processed samples has also increased compared to the base metal by 200 %. Despite these enhancements, corrosion resistance of new samples has decreased, which can be due to the numerous dislocations in the stress-induced stir zone, creating lattice deformations and causing the breakdown of the passive protective layer. The analysis of fracture surface topography through a Fractography method revealed a specific anaglyph consisting of dimples of various shapes, sizes, and dispersion and further confirmed the tensile test results.

1. Introduction

To create new materials, a thorough grasp of the link between material processing, structure, and attributes is required [1]. The demand for enhancing the mechanical characteristics of alloys has risen as technology and industry demands have evolved. The utilization of composites containing high-mechanical-property reinforcing particles has risen dramatically in recent years [2]. One of the most prevalent ways of composite manufacture is solid-state processing, which grinds the base metal and reinforcing particles without melting the material, resulting in increased mechanical qualities and corrosion resistance [3,4]. Aluminum-based composites are used in a variety of sectors. Because of their low density, high strength-to-weight ratio, and corrosion resistance, aluminum alloys are widely employed in the aerospace, military, and automotive sectors [5-10]. Aluminum alloy characteristics may be altered by using controlled procedures such as friction stir processing to incorporate additional particles, resulting in strong Aluminum-based composites [11]. Friction stir processing is a method for changing the characteristics of a surface without changing the properties of the underlying metal. It is based on the manufacture, processing, and synthesis of materials [12-15].

Aluminum alloys and composites are widely used by researchers in the engineering and material science field. In 2009, Yazdipour et al. [16] evaluated the influence of process parameters on the final grain size of Aluminum sheets by friction stir processing. They discovered that the process tool's quick cooling rate improves mechanical characteristics by improving the microstructure of the stirred zone. Additionally, lowering the tool's rotating speed while raising the advance speed minimizes grain size. In 2014, Khodabakhshi et al. [17] added Titanium dioxide particles to 5052 Aluminum alloy sheets in order to enhance their mechanical properties such as yield strength and elongation through friction stir processing. They could achieve this goal by refining the grain structure of the made composites after four passes of the process. They also claimed that increasing the number of passes eliminated agglomerates

and significantly improved ductility. In 2017, Rathee et al. [18] studied the penetration depth of the tool on the scattering pattern of reinforcing particles in the metal matrix. They reported that a lower penetration depth leads to insufficient heat production and the formation of holes, and a higher level of penetration depth causes the release of reinforcing particles and even the adhesion of materials to the tool shoulder. Therefore, for the production of composites with a defect-free surface, the optimal sinking depth is one of the essential parameters that must be considered. In 2019, Premnath [19] fabricated Al-SiC nanocomposites and intended to optimize friction stir parameters. These parameters included the number of passes, rotational speed, and forward feed of the tool. In doing so, he used the Taguchi method with a desirability approach. He reported that the number of passes is the determining parameter for tensile strength whereas rotational speed is the vital process parameter for microhardness. Higher values for tensile strength, improved microhardness and wear properties were achieved with 1500 rpm rotational speed and forward speed. In a similar work, Ikumapayi et al. [20] examined the improvements resulting from adding various reinforcement phases to Aluminum-based alloys and hybrid composites. They faced many challenges during the process of reaching the optimal parameters. They announced that a wide range of materials must be studied in order to obtain valid results.

The trend of the recent studies shows the importance of investigating different mechanisms and parameters of friction stir processing in the production of superior nanocomposites including aluminum-based composites.

In the current experimental study, several specimens of 6061T6 Aluminum alloy are provided and considered as the base metal. Then, three different composites made of these specimens are fabricated using friction stir processing. The first composite is processed without any powder, while for the other two composites, Alumina powders in micro and nano sizes are added as reinforcing particles. Between these composites and the base metal, mechanical properties (tensile strength, hardness, toughness, ductility, and failure mode) and corrosion resistance are analyzed and compared.

Finally, a Fractography method is used to investigate the effect of reinforcing particles on the type of fracture and the statistics of holes created.

The implemented Tools, methods, tests, and materials in this study will be explained in the following section.

2. Materials And Methods

According to the literature [21-24], adding ceramic particles to a metal can significantly reduce the ductility of the made composites. Therefore, to improve the ductility and reduce the hardness of the base alloy, a soft annealing process is performed on each specimen. In this process, the specimens are placed inside a furnace, and the temperature is raised from ambient to 420 °C and kept at this temperature for two hours. Then the heating is stopped, and the parts remain inside the furnace until the temperature reaches room temperature. This annealing process has reduced the hardness of the base alloy from 120 to 46 HV and prepared the specimens for friction stir processing.

To process and produce nano-composites, it is necessary to use two types of tools: Pin-less tools and pinned tools. The first tool has a conical shoulder with a diameter of 18 mm, which is necessary to close the holes containing the powder. The second tool is used to create the composite layer, and in addition to having a conical shoulder with a diameter of 18 mm, it includes a cylindrical pin with a sectional diameter of 5 mm and a length of 4.8 mm (the penetration depth). The tools used in this research are made of hot work steel H13, which was selected due to their high toughness and good abrasion resistance at high temperatures, as well as their good machinability. A vertical milling machine with a power of 1200 rpm is used to provide the required speed of the process.

Quantometer analysis of 6061T6 Aluminum alloy sheets is reported in Table 1. To improve the structure, nanometer/micrometer particles of alumina (500 nm and 4 μm) are used as reinforcing substances. Aluminum specimens with dimensions of 6 × 50 × 120 mm^3 are prepared and placed on the milling machine bed. Also, to add the alumina powder, holes with a diameter of 2 mm are created at specific distances from the moving tape of the parts. It should be noted that the linear hole pattern is used to fill the powder on the surface of the workpiece. Using the linear pattern on Aluminum specimens is for better surface mixing and uniform distribution of additives during the process.

Table 1

quantometer analysis of 6061-T6 Aluminum alloy.

6061T6 Aluminum alloy	Al %	Mg %	Si %	Fe %	Mn %	Zn %	Ti %	Cu %	Others
Standard	96-98	0.8	0.8	0.6	< 0.15	0.25	< 0.15	0.15-0.2	0.15
Present study	97.42	0.8	0.5	0.57	0.1	0.2	0.15	0.16	0.1

The clamping kits, the linear pattern on the specimens, and the implemented tools are shown in Figure 1. The parameters of friction stir processing are listed in Table 2.

Table 2

parameters of friction stir processing.

FSP Tools	Shoulder concavity angle ()	Tool shape	Tool deflection angle ()	Retention time (s)	Penetration depth (mm)	Feed rate ()	Rotational speed (rpm)
First tool	5	Conical shoulder without pin	3	0	0.2	50	1000
Second tool	5	Conical shoulder with a cylindrical pin	3	10	4.8 + 0.2	40	1200

One of the essential mechanical properties of the materials is the tensile strength, which determines the amount of stress tolerable by the part under tensile loads. In this study, tensile strength is considered as the response variable. Also, the corrosion of the stir zone of the processed samples is another critical parameter that needs to be investigated. The results of the tensile strength test can be used to extract the modulus of elasticity, final stress, fracture stress, percentage of elongation before fracture, toughness, and impact resistance. To investigate the tensile characteristics of the processed materials, a tensile strength test was performed on a small segment of the samples cut from the stir zone according to the ASTM-E8/E8M standard [25].

As seen in Figure 2, the samples are cut and prepared by the wire-cut machine (electrical discharge machine) to perform the tensile test in the direction of tool movement. After the tensile test, Fractography is performed on the surfaces of the fractured samples to observe the fracture mechanism. To measure the hardness of the samples, a Vickers-type microhardness test is performed on the surface of the composites. The load of the microhardness test is 200 g with 15 seconds of applying time, and the test is performed at every 3 mm distance on the surfaces. Because the applied force in this test is minimal and the reported microhardness is very sensitive to the quality of the surface, the samples should be polished according to the metallographic steps. On this basis, the samples are sanded with silicon carbide paper (3000 grit size) and then polished with 0.3 μm alumina abrasive powder by a polishing machine.

The electrochemical polarization test is carried out for these three composites and the base metal in a solution containing 3.5 weight percent NaCl with 60 minutes of immersion time based on the ASTM G5 standard. In this standard, a three-electrode system is used in a 3.5 % NaCl electrolyte medium. A Calomel electrode is selected as reference, Platinum as the counter electrode, and the evaluated sample as the working electrode.

The results of the tests and processes mentioned above will be discussed in the next section.

3. Results And Discussion

Elaborate details of the different tests done on the base metal and the three composites (without powder, with nanosized alumina, and with micronized alumina particles) are presented in this section. Tensile, hardness, and potentiodynamic polarization tests were carried out to examine the mechanical properties of these samples.

One of the concerns of this investigation is to control and reduce defects of the holes in the cross-section of the stir zone, which might be created during friction stir processing when low rotational speed and high forward speed are used. These defects were mainly observed at the beginning area of the workpiece, and the main reason is the low temperature of the tool and the sample during the process. Some defects could also be seen at the tail-end due to the tool coming out of the workpiece and the reduction of plastic materials in the leading part. The generated heat by low rotational speed and high forward speed, the

high thermal conductivity of Aluminum alloy, and the filling pattern are the main factors causing the poor fluidity of plastic materials around the tool. This, in turn, causes hole defects and leaves some cavities made by the leading tool unfilled. On this basis, rigorous attention was given to the performance of the process.

3.1. Tensile test

Results of the tensile test can be seen in Figure 3 as engineering stress/strain diagrams. Like other medium-ductile materials, these curves start with a linear elastic region followed by a strain hardening region, a necking region, and finally end at a fracture point. The linear part of the curves indicates that the specimens are perfectly aligned and fixed in the testing machine.

A typical 6061T6 Aluminum alloy has 12-17 % elongation at the fracture point. However here, after the annealing process, which made the base metal more ductile, the maximum elongation has reached 27.5 %. This value is 25.3 %, 20 %, and 19.3 % for powder-free, micro-alumina, and nano-alumina cases. These values indicate that the samples have become slightly brittle than the base metal after friction stir processing and even more brittle after adding alumina particles.

For the composite without any powder, the ultimate tensile strength is 178 MPa, and the yield strength is 88 MPa. This case has approximately 2.02 times higher strengths than the base metal. It is worth mentioning that the yield values reported here are computed as offset yield strength at 0.2 % of plastic strain. In the case of composite with micrometer reinforcing particles of alumina, the ultimate tensile strength is 186.6 MPa, and the yield strength is 83 MPa. These values are exactly two times higher than those of the base metal. For the last composite (with nano-alumina particles), the values of ultimate and yield strength are 134.98 and 57 MPa, respectively (1.41 times higher). The main reason for this enhancement is friction stir processing and the added ceramic particles. This process changes the material's microstructure by refining grain distribution and eliminating the defects and micro-voids through localized plastic deformation.

This enhancement is evident for the micro-alumina and without powder composites compared to the other two cases. Furthermore, micro-alumina composite shows an average of 42 % enhancement in strength compared to nano-alumina composite. This can be related to the large ceramic particles that can resist deformation more than nano-size particles.

The jagged regions on these curves are due to the heterogeneous changes in the structure of the samples under the test. Overall, the fabricated composites have more strength compared to the base metal.

Toughness is another characteristic of the materials that can be analyzed through a stress/strain diagram. Toughness is the ability of a material to absorb mechanical energy before the fracture and can be defined as the area under the stress/strain curves. According to the results, the toughness of the powder-free and micro-alumina samples are 76 % and 36 % higher than the base metal. On the other hand, the toughness of the nano-alumina sample has decreased by 4.5 % compared to the base metal.

The reduction of the latter case is because this case has become relatively more brittle than the base metal despite an increase in strength.

Based on the results of the tensile test, from a manufacturing point of view, if higher strengths and yet suitable ductile composites of 6061-T6 Aluminum alloy are needed, only friction stir processing is suggested with no additives. With this process, the strength of this alloy can increase by 202 % with only a slight decrease in ductility (8.6 %).

3.2. Hardness test

Hardness is another tribological characteristic of a material that can be defined as the resistance against localized plastic deformation. Hard materials tend to have high strength, and by the data analyzed in the previous section, it can be easily understood that the fabricated composites have higher hardness than the base metal. Nevertheless, to investigate in detail, a pressing-in method is used to calculate the hardness of these four specimens.

A transversal segment of the base metal and the made composites is selected to measure and compare the hardness properties, as shown in Figure 4 (a). Eleven indentation spots on this segment at every 3 mm distance from the center of the stir zone are determined for the test report points. The hardness of the samples in the stir zone is affected by the size of reinforcing particles in different areas. Figure 4 (b) presents the hardness changes based on the Vickers test for all cases. The hardness profile of the base metal is more uniform than the profiles of processed samples. The grain refinement of composite samples is due to friction stir processing and the relatively consistent presence of alumina particles, which act as the nucleus and prevent grain growth during recrystallization [26]. By examining the hardness of the samples before and after the process, it is observed that the hardness has increased in all processed cases. The associated reasons for this increase can be stated as follow:

- Grain refinement during recrystallization,
- Elimination of the defects and micro-voids of the alloy by compression of friction stir processing tool,
- Localized plastic deformation,
- Alumina particles, having harder phases, are uniformly distributed in the Aluminum field and form a particle-reinforced composite.

The trend of these curves shows the impact of friction stir processing on the hardness properties. As can be seen, the highest average hardness is obtained for three processed samples, which is equivalent to 96 HV. This value is 2 times higher than the base case (48 HV). Overall, this test shows that friction stir processing and the addition of alumina reinforcing particles have a positive effect on the hardness behavior of the samples.

The results of the tensile and hardness analysis can be summarized as follow:

- The yield and ultimate tensile strength of the processed samples have increased compared to the unprocessed base metal. In general, the strength of this alloy will increase regardless of the presence or absence of reinforcing particles after applying friction stir processing.
- The samples' flexibility after friction stir processing has been reduced.
- The micro-alumina composite showed more tensile and ultimate strength than the nano-alumina sample. In addition, with an almost equal level of ductility, the micro-alumina sample gained more toughness as opposed to the nano-alumina case.
- The processed samples became harder compared to the base alloy. In general, the hardness of 6061T6 Aluminum alloy will increase in the presence or absence of reinforcing particles after friction stir processing.

3.3 corrosion test

A small segment of the specimens is selected for the corrosion test, perpendicular to the stir zone with dimensions of 10 × 10 × 6 mm^3. Before the test, the samples are polished with sandpaper and degreased with acetone. After washing with distilled water, except on the intended surface, the rest are covered with varnish. Then, to quantify the samples' response to corrosion, a corrosion test is performed with 60 minutes of immersion time in 3.5 weight percent NaCl solution (pH = 7) according to the standard of the ASTM G5 electrochemical corrosion test. In this test, Calomel is selected as the reference electrode, Platinum as the counter electrode, and the samples as the working electrodes.

The weight of the samples was measured before and after the corrosion test. The weight loss of the samples is an indicator of the corrosion rate.

The current produced in an electrochemical cell when corrosion occurs is known as the corrosion current. The flow of electrons from the anode (oxidation region on the surface) to the cathode (reduction region at inner layers) is referred to as electrochemical corrosion. An electric current is generated in the system by passaging electrons from the electronegative to the more electropositive regions. When electrons are lost at the anode, oxidation reactions occur, causing the anode to degrade (corrode) while the cathode is untouched. The size of the corrosion current is proportional to the potential difference in the system. That is, the more significant the potential difference, the higher the corrosion current generated, and hence the more severe the anode corrosion rate. Furthermore, Corrosion resistance is a metal's ability to retain its binding energy and withstand the degradation and chemical breakdown that would otherwise occur during the corrosion.

The corrosion behavior of all cases is shown in Figure 5. These potentiodynamic polarization curves are obtained using VersaSTAT4 software. In addition, the electrochemical parameters calculated from these curves are listed in Table 3, along with the corrosion rate and resistance.

The quantities of corrosion current density, corrosion potential, and anodic and cathodic Tafel slopes were calculated by drawing two tangential lines on the cathodic and anodic curves and one horizontal

line from the point where the two curves meet. The horizontal coordinate of the attained intersecting point denotes the corrosion current value, and the vertical coordinate indicates the magnitude of corrosion potential.

The corrosion rates were calculated for the tested samples based on the weight loss method, which can be defined as the amount of thickness loss due to corrosion each year ($^{mm}/_{yr}$) [27].

Lower corrosion current density denotes a lower rate of corrosion. According to the results of figure 5 and table 3, the base metal has the lowest value of corrosion current density and corrosion rate and therefore is more resistant to corrosion than other cases. Interestingly, friction stir processing has significantly decreased the corrosion resistance of the processed samples. This degrading behavior of friction stir processing towards corrosion was also mentioned in the works of [28] and [29]. This behavior might be due to the numerous dislocations in the stress-induced stir zone, which causes lattice deformations. The solution would permeate these localized flaws, causing the protective layer to break down and produce localized corrosion.

It is observed that by applying two processing passes to the alloy, the values of corrosion current and corrosion rate increase, and the corrosion resistance decreases.

Table 3

Electrochemical parameters of polarization corrosion.

	Anodic Tafel Slope	Cathodic Tafel Slope	Corrosion Resistance	Corrosion Potential	Corrosion Current	Corrosion Rate
Base metal	0.11	0.14	1390	-1.02		0.22
Nano-alumina	0.18	0.11	512.3	-1.42		0.61
Powder-free	0.13	0.091	373.4	-1.43		0.72
Micro-alumina	0.22	0.1	362.9	-1.434		0.84

3.3.1 Polarization behavior

In the anodic branch of the diagram, the corrosion current increases abruptly due to the presence of a top layer on the alloy surface. In contact with the corrosive environment, some active metals suddenly become incredibly resistant to corrosion. This is due to a phenomenon called chemical passivation. In these situations, the metal goes through a reaction and creates a layer of very thin corrosion products that is invisible and is a complete barrier that reduces corrosion by several orders of magnitude [30]. In

the case of Aluminum and its alloys, a sticky oxide layer is slowly formed when the alloy is exposed to the air. This adhesive oxide layer on the surface causes corrosion resistance in Aluminum alloys. Considering all four samples, the corrosion resistance can be expressed as follow:

Base metal > Nano-alumina > Powder-free > Micro-alumina

According to the electrochemical corrosion test, the base metal is approximately 342 % more resistant to corrosion than the other composites. The powder-free and micro-alumina composites show almost a similar corrosion behavior, while the nano-alumina composite results in 41 % higher corrosion resistance compared to the other two composites.

3.3 Fracture analysis

The fracture mechanism of the samples after the tensile test is discussed in this section. A ductile fracture occurs in metals with profound ductility and high toughness, such as Aluminum. It begins with germination, growth, and fusion of micro-holes near the cross-sectional center of the sample under tensile stress. Void creation and coalescence, crack propagation, and failure are the main processes in ductile fracture, which commonly result in a cup-and-cone-shaped failure surface. Microscopically, voids usually form in the material around inclusions, secondary phases, and grain boundaries. On the other hand, in brittle fracture, there is more minor degree of plastic deformation and energy absorption before the failure.

Fractography images of the fracture surfaces are shown in Figure 6 for all cases. It can be understood from figures 6(a) and (b) that the base metal and the powder-free sample have failed softly during the tensile test. Large and deep dimples, large shear-cut edges, and the roughness visible in these figures are characteristics of the ductile fracture. For the micro and nano-alumina samples, small and shallow depressions, as well as a multitude of cleavage surfaces, can be seen in figures 6(c) and (d), which indicate a low/limited ductility failure class. For these two composites with additives, the inclusion density influences the nucleation rate of micro-voids, resulting in a more significant number of nucleation sites and lesser growth potential. This, in turn, leads to a high void distribution density and more minor size dimples, indicating reduced overall ductility. The Fractography images of fracture surfaces confirm the results of the tensile test that was presented in section 3.1.

4. Conclusion

The mechanical properties and corrosion behavior of 6061T6 Aluminum alloy and three fabricated composites from this alloy were experimentally investigated in this paper. The composites were made during two passes of friction stir processing. Alumina powder () was used as reinforcing particles. These composites included a powder-free sample, a micro-alumina sample, and a nano-alumina sample. The hardness, tensile, and Potentiodynamic polarization tests were performed to compare the new samples with the base metal. In addition, Fractography images of fractured surfaces were used to confirm the failure mode of the samples and the results reported by the tensile test.

Based on the research conducted in this study, the following conclusions can be obtained:

- The tensile tests show that friction stir processing has increased the tensile and ultimate strength of the composites by an average of 181% compared to the base metal. Applying friction stir processing changes the material's microstructure by refining grain distribution and eliminating the defects and micro-voids. The strength of the composites with additives is affected by the size of the particles, as the micro-alumina sample shows 42 % higher strength than the nano-alumina sample.
- The processed samples have become harder than the base alloy by 200 %. In general, the hardness of 6061T6 Aluminum alloy increases in the presence or absence of reinforcing particles after friction stir processing.
- The corrosion resistance of new samples has decreased, which can be due to the numerous dislocations in the stress-induced stir zone, creating lattice deformations and causing the breakdown of the passive protective layer. Nano-alumina sample is 41 % more resistant to corrosion than the micro-alumina composite.
- Fractography images of the fracture surfaces show a ductile fracture mode for the base metal and the powder-free sample with large and deep dimples and large shear-cut edges. However, For the micro and nano-alumina samples, small and shallow depressions as well as a multitude of cleavage surfaces were observed, which indicate a low/limited ductility failure class.
- When choosing between microparticles or nanoparticles for the production of Aluminum-based composites, the application's necessities should be considered. There is a clear trade-off between the strength and the corrosion properties of these materials. The micro-alumina composite has 42 % higher strength while 41 % less corrosion resistance than the nano-alumina composite.

Declarations

Data availability

The raw/processed data required to reproduce these findings cannot be shared at this time as the data also forms part of an ongoing study

Competing interests

The authors declare no competing interests.

References

[1] P. Ravindran, K. Manisekar, P. Rathika, P. Narayanasamy, Tribological properties of powder metallurgy – Processed Aluminum self-lubricating hybrid composites with SiC additions, J. Materials and Design 2013; 45: 561-570.

https://doi.org/10.1016/j.matdes.2012.09.015

[2] B. S. Yigezu, P. K. Jha, M. M. Mahapatra, The Key Attributes of Synthesizing Ceramic Particulate Reinforced Al-Based Matrix Composites through Stir Casting Process: A Review, J. Materials and Manufacturing Processes 2013; 28(9): 969-979.

DOI: 10.1080/10426914.2012.677909

[3] V. V. Monikandan, M. A. Joseph, P. K. Rajendrakumar, Dry sliding wear studies of Aluminum matrix hybrid composites, J. Resource-Efficient Technologies 2016; 2: S12-S24.

https://doi.org/10.1016/j.reffit.2016.10.002

[4] ASTM E8/ E8M-21, Standard Test Methods for Tension Testing of Metallic Materials, ASTM International, West Conshohocken, PA, 2021.

https://standards.globalspec.com/std/14376655/ASTM%20E8/E8M-21

[5] R. I. M. Asri, W. S. W. Harun, M. Samykano, N. A. C. Lah, S. A. C. Ghani, F. Tarlochen, M. R. Raza, Corrosion and surface modification on biocompatible metals: A review, J. Material Science and Engineering: C 2017; 77: 1261-1274.

https://doi.org/10.1016/j.msec.2017.04.102

[6] C. Zhang, Z. Ding, L. Xie, L-C. Zhang, L. Wu, Y. Fu, L. Wang, W. Lu, Electrochemical and in vitro behavior of the nanosized composites of Ti-6Al-4V and fabricated by friction stir process, J. Applied Surface Science 2017; 423: 331-339.

https://doi.org/10.1016/j.apsusc.2017.06.141

[7] Y. Cao, H. Ayed, S. Jafarmadar, M. A. A. Abdollahi, A. Farag, M. Wae-hayee, M. Hashemian, PEM fuel cell cathode-side flow field design optimization based on multi-criteria analysis of liquid-slug dynamics, Journal of Industrial and Engineering Chemistry 98 (2021) 397-412.

https://doi.org/10.1016/j.jiec.2021.03.024

[8] G. M. Ludtka, D. E. Laughlin, The influence of microstructure and strength on the fracture mode and toughness of 7XXX series aluminum alloys, J. Metallurgical Transactions A 1982; 13: 411-425.

https://doi.org/10.1007/BF02643350

[9] F. Hannard, S. Castin, E. Maire, R. Mokso, T. Pardoen, A. Simar, Ductilization of aluminum alloy 6056 by friction stir processing, J. Acta Materialia 2017; 130: 121-136.

https://doi.org/10.1016/j.actamat.2017.01.047

[10] M. A. A. Abdollahi, S. Jafarmadar, A. Jabbary, S. R. Amini Niaki, Effect of cathode-side gas flow channels section geometry on the removal process of liquid slug in a proton exchange membrane fuel cell, Proceedings of the Institution of Mechanical Engineers, Part E: Journal of Process Mechanical Engineering. March 2022.

https://doi.org/10.1177/09544089221086391

[11] A. Kurt, I. Uygur, E. Cete, Surface modification of Aluminum by friction stir processing, J. Materials Processing Technology 2011; 211.3: 313-317.

https://doi.org/10.1016/j.jmatprotec.2010.09.020

[12] F. Khan MD, G. M. Karthik, S. K. Panigrahi, G. D. Janaki Ram, Friction stir processing of QE22 magnesium alloy to achieve ultrafine-grained microstructure with enhanced room temperature ductility and texture weakening, J. Mater. Char. 2019; 147: 365-378.

https://doi.org/10.1016/j.matchar.2018.11.020

[13] Z. Shen, Y. Ding, A. P. Gerlich, Advances in friction stir spot welding, J. Crit. Rev. Solid State Mater. Sci. 2019; 45(6): 457-534.

https://doi.org/10.1080/10408436.2019.1671799

[14] A. H. Feng, B. L. Xiao, Z. Y. Ma, R. S. Chen, Effect of friction stir processing procedures on microstructure and mechanical properties of Mg-Al-Zn casting, J. Metall. Mater. Trans. A 2009; 40: 2447-2456.

https://doi.org/10.1007/s11661-009-9923-0

[15] R.S. Mishra, Z.Y. Ma, I. Charit, Friction stir processing: a novel technique for fabrication of surface composite, J. Materials Science and Engineering: A 2003; 341: 307-310.

https://doi.org/10.1016/S0921-5093(02)00199-5

[16] A. Yazdipour, A. Shafiei, K. Dehghani, Modeling the microstructural evolution and effect of cooling rate on the nanograins formed during the friction stir processing of Al5083, J. Material Science and Engineering: A 2009; 527(1-2): 192-197.

https://doi.org/10.1016/j.msea.2009.08.040

[17] F. Khodabakhshi, A. Simchi, A. H. Kokabi, M. Sadeghahmadi, A. P. Gerlich, Reactive friction stir processing of AA 5052- nanocomposite: process-microstructure-mechanical characteristics, J. Material Science and Technology 2014; 426-435.

https://doi.org/10.1179/1743284714Y.0000000573

[18] S. Rathee, S. Maheshwari, A. N. Siddiquee, M. Srivastava, Effect of tool plunge depth on reinforcement particles distribution in surface composite fabrication via friction stir processing, J. Defence Technology 2017; 13.2: 86-91.

https://doi.org/10.1016/j.dt.2016.11.003

[19] A. Premnath, Optimization of the process parameters on the mechanical and wear properties of Al-SiC nanocomposites fabricated by friction stir processing using desirability approach, J. Silicon 2019; 12: 665-675.

https://doi.org/10.1007/s12633-019-00178-6

[20] O. M. Ikumapayi, E. T. Akinlabi, S. K. Pal, J. D. Majumdar, A survey on reinforcements used in friction stir processing of aluminium metal matrix and hybrid composites, J. Procedia Manufacturing 2019; 35: 935-940.

https://doi.org/10.1016/j.promfg.2019.06.039

[21] R. D. Bourkhani, A. R. Eivani, H. R. Nateghi, Through-thickness inhomogeneity in microstructure and tensile properties and tribological performance of friction stir processed AA1050- nanocomposite, J. Compos. B Eng. 2019; 174: 107061.

https://doi.org/10.1016/j.compositesb.2019.107061

[22] I. Charit, R. S. Mishra, Abnormal grain growth in friction stir processed alloys, J. Scripta Materialia 2008; 58(5): 367-371.

https://doi.org/10.1016/j.scriptamat.2007.09.052

[23] S. M. Ma, P. Zhang, G. Ji, Z. Chen, G. A. Sun, S. Y. Zhong, V. Ji, H. W. Wang, Microstructure and mechanical properties of friction stir processed Al-Mg-Si alloys dispersion-strengthened by nanosized Ti particles, J. Alloys Compd. 2014; 616: 128-136.

https://doi.org/10.1016/j.jallcom.2014.07.092

[24] H. B. M. Rajan, I. Dinaharan, S. Ramabalan, E. T. Akinlabi, Influence of friction stir processing on microstructure and properties of AA7075/Ti in situ composite, J. Alloys Compd. 2016; 657: 250-260.

https://doi.org/10.1016/j.jallcom.2015.10.108

[25] ASTM E8/ E8M-13a, Standard Test Methods for Tension Testing of Metallic Materials, AASHTO No.: T68. West Conshohocken, PA 19428-2959. United States.

https://www.galvanizeit.com/uploads/ASTM-E-8-yr-13.pdf

[26] M. Raaft, T. S. Mahmoud, H. M. Zakaria, T. A. Khalifa, Microstructural, mechanical and wear behavior of A390/graphite and A390/ surface composites fabricated using FSP, J. Materials Science and Engineering: A 2011; 528: 5741-5746.

https://doi.org/10.1016/j.msea.2011.03.097

[27] D. S. Rao, N. Ramanaiah, Evaluation of Wear and Corrosion Properties of AA6061/ Composites Produced by FSP Technique, J. Minerals and Materials Cha. and Eng. 2017; 5: 353-361.

https://doi.org/10.4236/jmmce.2017.56029

[28] X. Wang, Y. Li, Y. Hou, H. Bian, Y. Koizumi, A. Chiba, Effect of surface friction treatment on the in vitro release of constituent metals from the biomedical Co-29Gr-6Mo-0.16N alloy, J. Material Science and Engineering: C 2016; 64: 260-268.

https://doi.org/10.1016/j.msec.2016.03.050

[29] H. R. Lashgari, C. Kong, M. Asnavandi, Sh. Zangeneh, The effect of friction stir processing (FSP) on the microstructure, nanomechanical and corrosion properties of low carbon alloy, J. Surface and Coating Technology 2018; 354: 390-404.

https://doi.org/10.1016/j.surfcoat.2018.09.039

[30] Q. Xing, S. Renguo, Q. Wenjuan, J. Jirong, W. Chao, L. Hai, X. Ying, Consistent variation of stress corrosion cracking susceptibility and passive film-induced stress for 7050 Aluminum alloy with polarization potential, J. Rare Metal Materials and Engineering 2016; 45(8): 1943-1948.

https://doi.org/10.1016/S1875-5372(16)30151-5

Figures

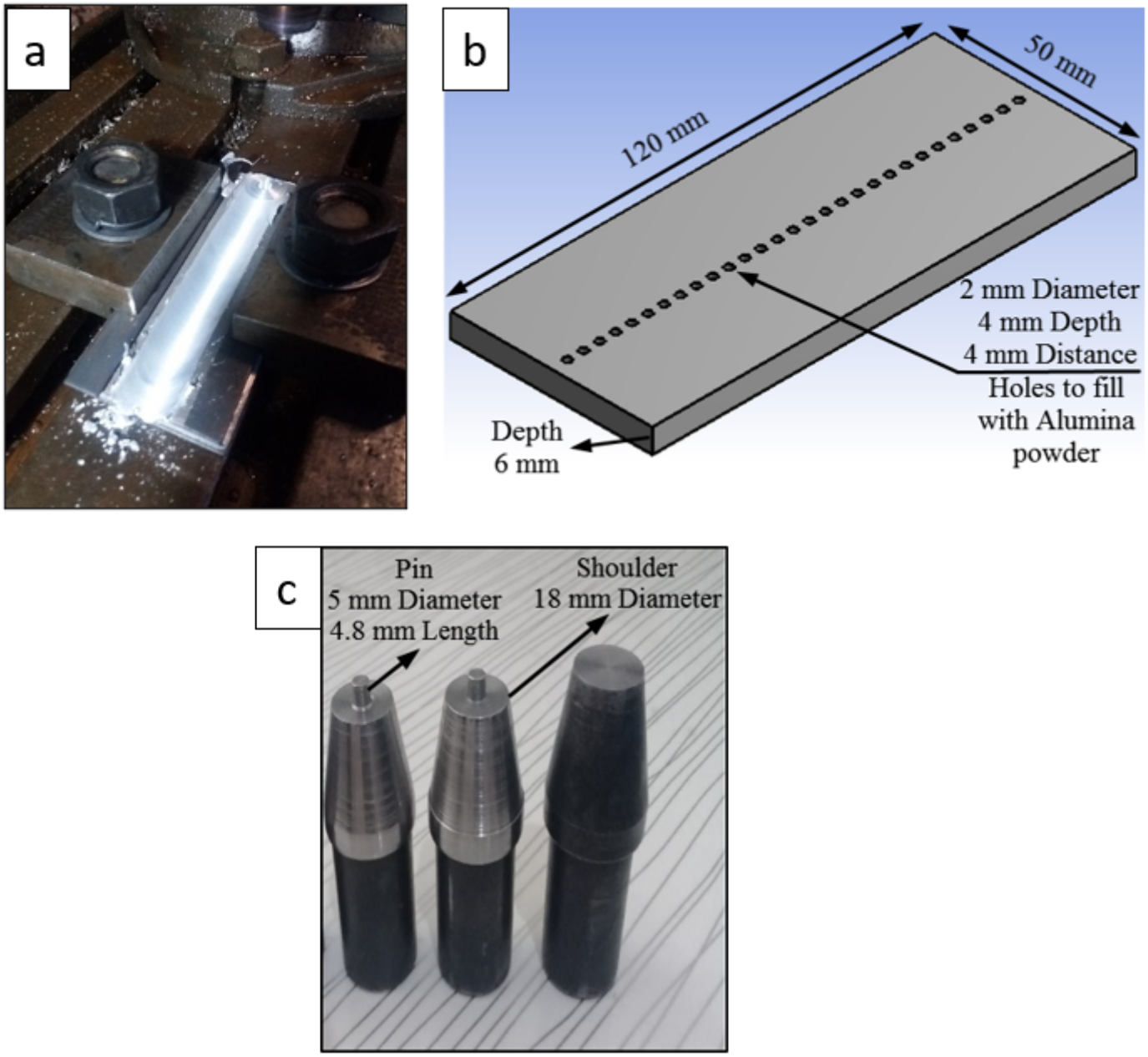

Figure 1

a) The image of processing and fixtures to hold the workpiece, b) Linear hole pattern for powder filling, c) Tools used in the present study.

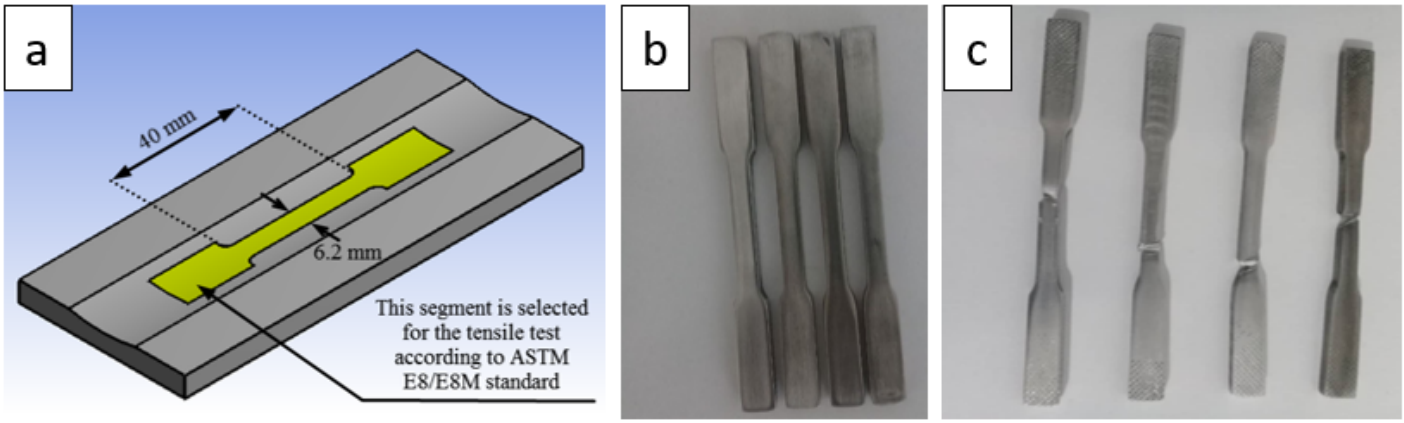

Figure 2

Dimensions of the tensile specimens a) According to ASTM E8/E8M standard [25], b) Before the tensile test, c) After the tensile test.

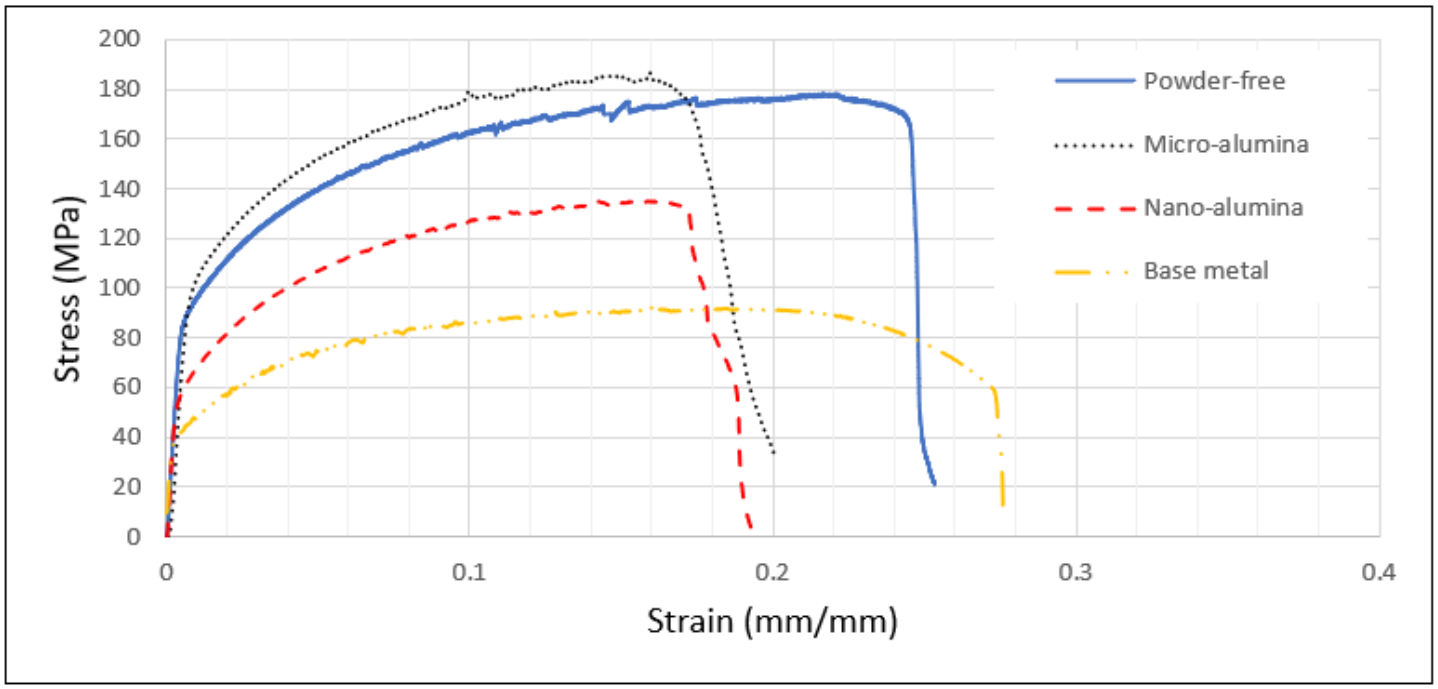

Figure 3

Engineering Stress/strain diagram of the base metal and the composites.

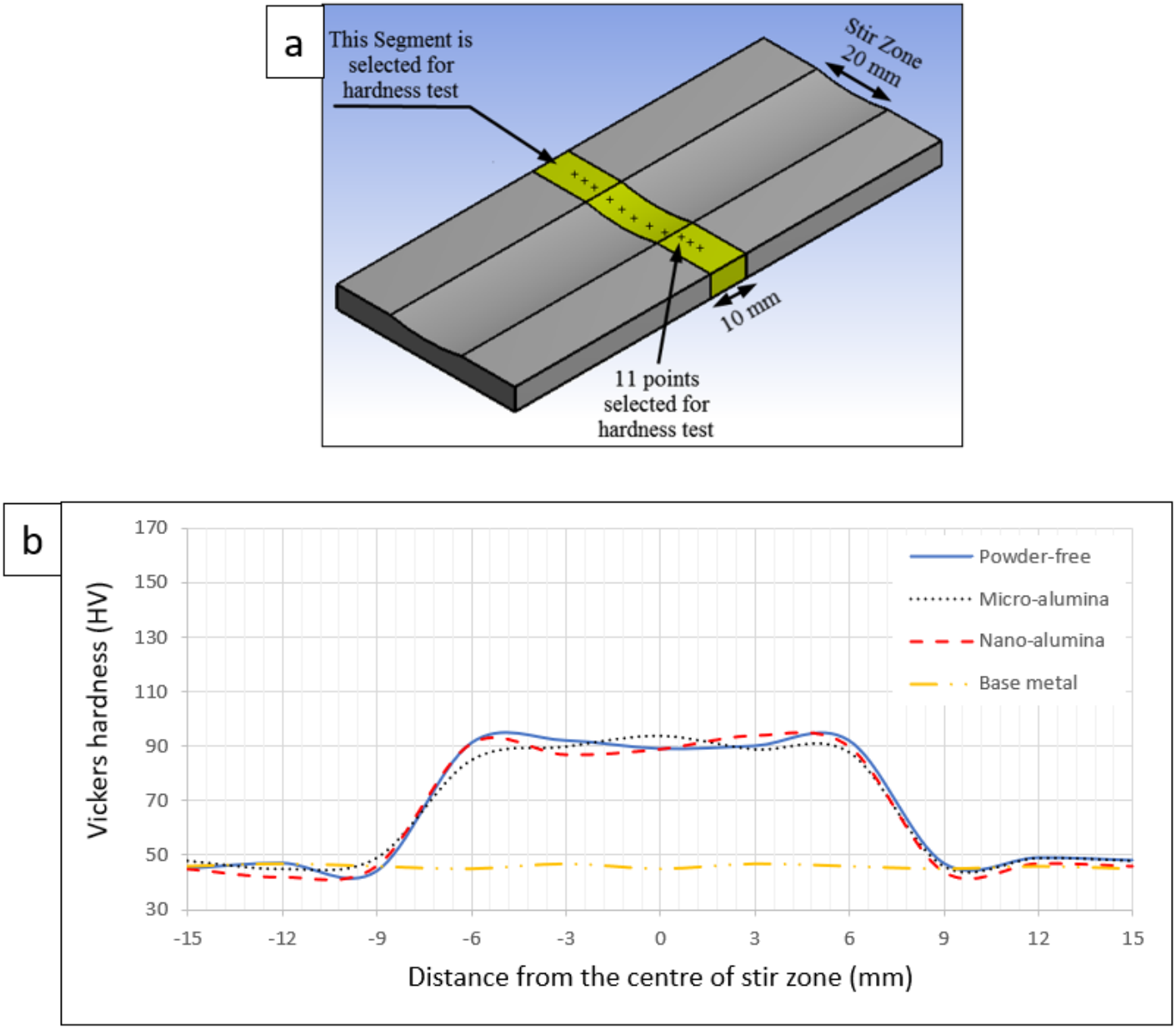

Figure 4

a) Schematic representation of hardness spots, b) Hardness test results of the base metal and the processed samples.

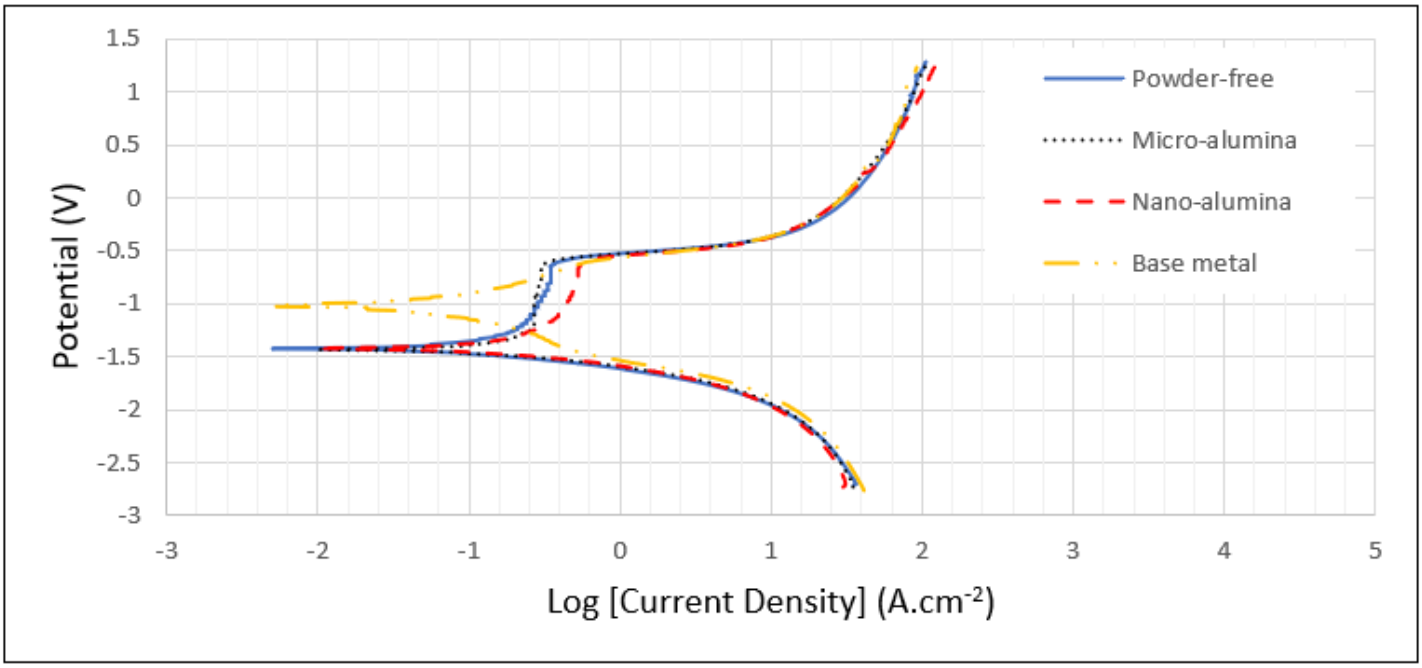

Figure 5

Potentiodynamic polarization curves of all cases.

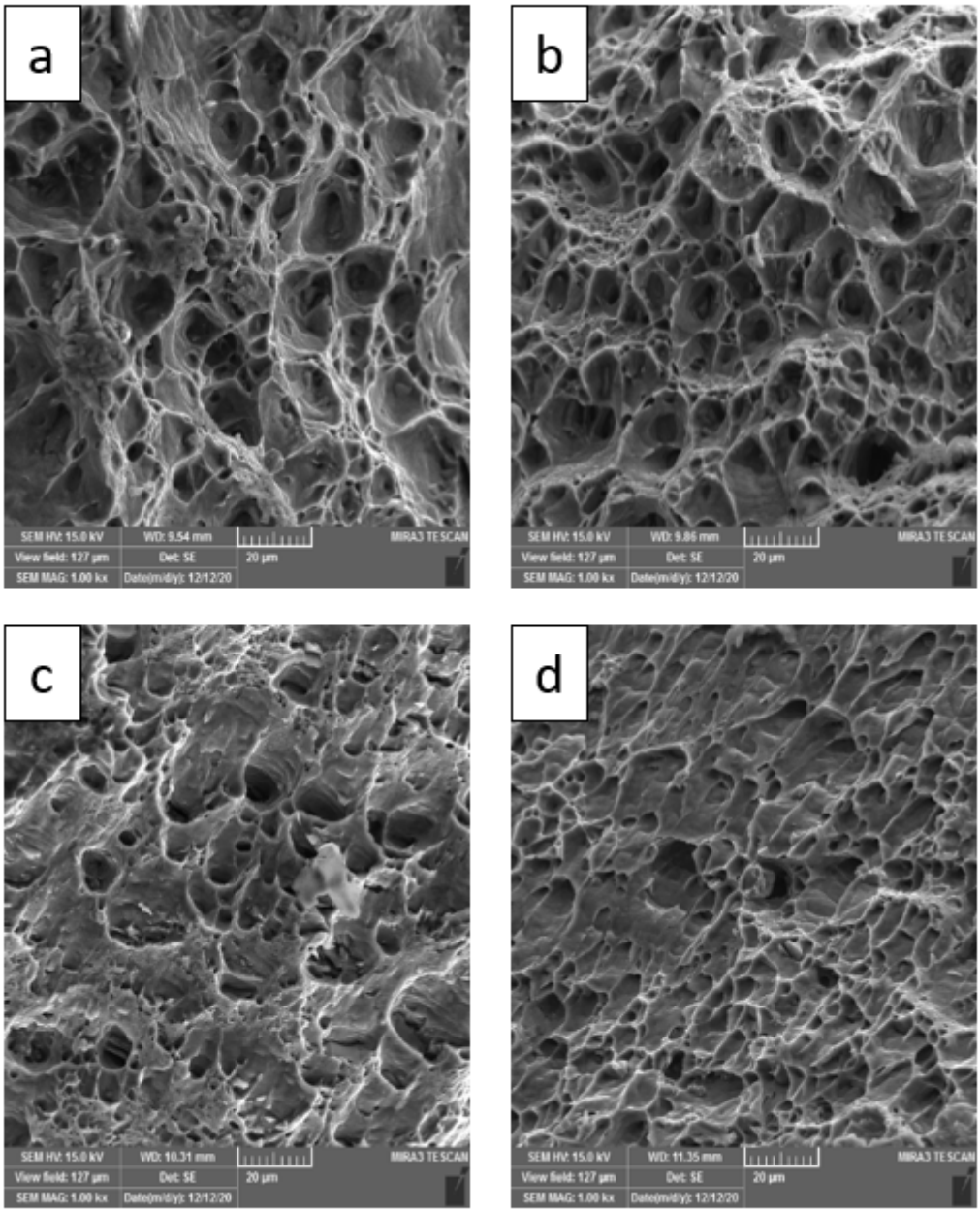

Figure 6

Fractography images of the fracture surface a) base metal, b) powder-free sample, c) micro-alumina sample, d) nano-alumina sample.